Direct Measurements of Heterotypic Adhesion between the Cell Surface Proteins CD2 and CD48[†]

Boru Zhu,[‡] Elizabeth A. Davies,[§] P. Anton van der Merwe,*[,§] Tammy Calvert,[‡] and Deborah E. Leckband*[,‡,||]

Departments of Chemical Engineering and Biochemistry, University of Illinois at Urbana−Champaign, Urbana, Illinois 61801, and Sir William Dunn School of Pathology, University of Oxford, OX1 3RE Oxford, U.K.

Received April 22, 2002; Revised Manuscript Received August 1, 2002

ABSTRACT: Direct force measurements were used to investigate the molecular mechanism of heterophilic adhesion between the murine T-cell adhesion glycoprotein CD2 and its ligand CD48. From the distance dependence of the protein−protein interaction potential, we demonstrate directly that the full-length extracellular domains adhere in a head-to-head orientation. The absence of long-range electrostatic protein−protein attraction further indicates that the salt bridges between the binding surfaces only influence the interaction at short range. Despite the loss of a stabilizing disulfide bond in domain 1 (D1) of CD2, adhesive failure occurs abruptly with no evidence of partial protein unfolding during detachment. Finally, these measurements between extended membrane surfaces directly confirm that the low-affinity CD2−CD48 bond generates weak adhesion and that lateral receptor mobility is required for the development of appreciable adhesion. This is the first direct measurement of the range and magnitude of the forces governing heterotypic adhesion mediated by cell surface proteins. These results both verified the head-to-head CD2−CD48 docking alignment and demonstrated the ability to elucidate the structure−function relationships of adhesion proteins from the measured distance dependence of their interaction potentials.

CD2, a glycoprotein on the T lymphocyte plasma membrane (*1*−*3*), is the first cell adhesion molecule demonstrated to undergo heterophilic recognition in cell−cell adhesion (*4*). It is now well established that the ligands for CD2 are CD48 in mice or rats (*1*, *5*, *6*) and CD58 (LFA-3)[1] in humans (*7*−*9*). The structure comparisons suggested that CD2, as well as its counterparts CD48 and CD58, belongs to the immunoglububin superfamily (*10*, *11*). CD2 binding to its ligands was found to have exceptionally fast dissociation rate constants, which result in low affinities (*1*, *12*−*14*).

The mechanism of binding was suggested by the crystal structures of the soluble, extracellular region of CD2, which revealed a homodimeric head-to-head crystal contact with an area of 650−690 Å^2 (*15*, *16*). There are no reports of homophilic CD2 interactions, but the head-to-head association was proposed as a possible model for CD2 interactions with its ligands. The CD2−ligand complex was thus predicted to span an intermembrane gap of 135 Å, which is identical to that spanned by MHC and its ligand, the TCR. NMR analysis of interacting soluble forms of CD2 and CD48 (*17*), as well as the crystal structure of the complex of CD2 D1 and CD 58 D1, further supports this view (*18*, *19*). Nevertheless, despite the compelling evidence, this model for adhesion has not been directly verified.

The kinetics of CD2 binding is also distinguished by its rapid dissociation from its ligands CD48 and CD58 (LFA-3), which approach rates of 7−8 s^{-1} (*20*). This raises the question as to the adhesiveness of these proteins relative to that of other adhesion proteins. The functional significance of the fast off-rates is thought to allow cells to rapidly form and break contacts. This has obvious advantages, especially with regard to conferring plasticity at cell−cell contacts or enabling the rapid surveillance of target membranes. Experimental studies done with CD58 (LFA-3) and CD2 indicate that the rapid receptor−ligand dissociation is responsible for high receptor and ligand mobility at cell−cell contacts (*21*−*23*). A recent theoretical study showed that the kinetics of receptor−ligand binding determine the dynamics of assembly of distinct receptor−ligand patterns at intercellular junctions (*24*).

The relationship between rapid dissociation rates and adhesion involving multiple bonds in parallel is less clear.

[†] Supported by NIH Grant GM51338 (D.E.L.) and by the U.K. Medical Research Council (P.A.v.d.M.).

* Address correspondence to these authors. D.E.L.: Department of Chemical and Biomolecular Engineering, 600 S. Mathews Ave., Urbana, IL 61801. Tel: 217-244-0793. Fax: 217-333-5052. E-mail: leckband@scs.uiuc.edu. P.A.v.d.M.: Sir William Dunn School of Pathology, University of Oxford, OX1 3RE Oxford, U.K. Tel: 44-01865-275593. Fax: 44-01865-275591. E-mail: anton.vanderMerwe@pathology.oxford.ac.uk.

[‡] Department of Chemical and Biomolecular Engineering, University of Illinois at Urbana−Champaign.

[§] University of Oxford.

[||] Department of Biochemistry, University of Illinois at Urbana−Champaign.

[1] Abbreviations: DLPC, 1,2-dilauroylphosptidylcholine; NTA-DLGE, 6-[9-[2,3-bis(dodecyloxy)propyl]-3,6,9-trioxanonyl-1-oxycarboxylamino]hexanoic acid dilauroylglycerol ester; DSIDA, distearoyl glyceryl ether iminodiacetic acid; DPPE, 1,2-dipalmitoylphosphatidylethanolamine; DSPC, 1,2-distearoylphosphatidylcholine; DTPC, 1,2-ditridecanoylphosphatidylcholine; FITC, fluorescein isothiocyanate; MOPS, 3-(*N*-morpholino)propanesulfonic acid; SFA, surface force apparatus; LFA-3, leukocyte function-associated molecule 3; IgSF, immunoglobulin superfamily; SPR, surface plasmon resonance; LB, Langmuir−Blodgett; JKR, Johnson−Kendall−Roberts; TCR, T-cell receptor; APC, antigen-presenting cell; MHC, major histocompatibility complex; NMR, nuclear magnetic resonance.

10.1021/bi020296g CCC: $22.00
Published on Web 09/06/2002

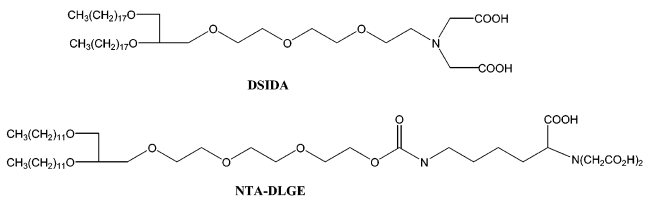

FIGURE 1: Molecular structures of the two chelating lipids, DSIDA and NTA-DLGE, used in these studies.

There is increasing evidence that, in the absence of rebinding, the strengths of stressed, *isolated* bonds far from equilibrium are determined by the activation energies for unbinding, the position of the transition state, and the rate of pulling (*25*, *26*). A similar analysis does not, however, exist for multiple bonds in parallel. One significant difference in the latter case is that, under near-equilibrium conditions, bonds can break and re-form many times before the adhesive junction fails. This dynamic exchange will affect the measured adhesion (*27*). Seifert determined how the force scales with the number of bonds in parallel and also demonstrated that the dependence on loading rate differs from single bond behavior (*28*). Under equilibrium loading conditions, the adhesive force is the maximum gradient in the intersurface potential. The limitation of theoretical analyses developed thus far to describe multiple bond behavior is that they do not cover a sufficiently wide range of loading rates to address both near- and far-from-equilibrium behavior (*27*, *28*). Thus, the link between kinetics, the thermodynamic properties of the bonds, and adhesion has not been established.

This report describes direct surface force measurements of the range and magnitude of interactions between membranes displaying rat CD2 and CD48. The high, absolute distance resolution of the surface force apparatus enabled us to establish directly that the full-length proteins adhere in a head-to-head alignment. Direct force measurements were conducted between proteins on extended membrane surfaces, which is more representative of a cell membrane than isolated receptor−ligand pairs. This facilitated investigations of the collective adhesive behavior of multiple receptor−ligand bonds in parallel and the requirement of lateral mobility for generating detectable adhesion mediated by the low-affinity CD2−CD48 bonds.

MATERIALS AND METHODS

Chemicals. The nickel chelating lipid, NTA-DLGE, and the copper chelating lipid, DSIDA, were from Northern Lipids (Vancouver, Canada). The molecular structures of both lipids are shown in Figure 1. DPPE, DSPC, and DTPC were from Avanti Polar Lipids (Alabaster, AL). FITC-labeled DPPE was purchased from Molecular Probes (Eugene, OR). MOPS and all salts used in the study were purchased from Sigma. Aqueous solutions were prepared with water purified with a Milli-Q UV filtration system (18 MΩ resistance, Millipore).

Protein Preparation. Soluble forms of murine CD2 and CD48 with C-terminal oligohistidine tags were expressed in Chinese hamster ovary cells and purified using Ni-NTA−agarose, as described for sCD80 (*6*, *29*). The C-terminal 12 residues of CD2 and CD48 were VNCPEKHHHHHH and PCDLARHHHHHH, respectively. Both proteins were purified by gel filtration on a Superdex S75 FPLC column. Their elution position was consistent with their being monomeric in solution. The activities of CD2 and CD48 were tested in measurements of their binding affinity with a BIAcore surface plasmon resonance instrument, as previously described (*6*). Both proteins were shown to be stable under the transport and experimental conditions used.

Force Measurements. Force measurements were conducted with a Mark II SFA in a temperature-controlled room at 25 ± 1 °C. The SFA was interfaced with a Jarrell Ash imaging spectrometer and a video recording system. The SFA quantifies the normalized force between materials on the surfaces of two macroscopic, crossed hemicylindrical silica lenses as a function of their separation distance (*30*). The absolute intersurface distance is determined with a resolution of ±1 Å by optical interferometry (*31*). The force between the surfaces is determined within ±1 nN from the deflection of a sensitive spring, which is attached to one of the two lenses supporting the samples (*30*). Importantly, for geometries where the radius R is greater than the range of the interaction ($R \gg D$), as in these measurements ($R = 2$ cm), the total force between the two macroscopic curved surfaces $F_c(D)$ is related to the interaction energy per area $E_f(D)$ between two equivalent flat plates by $F_c(D)/R = 2\pi E_f(D)$. This is the well-known Derjaguin approximation (*32*) and is derived in several standard textbooks (*33*, *34*). The SFA measurements thus yield the interaction potential between the surfaces, and the geometry only influences the measurements through the scaling factor $2\pi R$. This applies for any arbitrary interaction potential $E(D)$ or force law $F(D) = -dE/dD$ (*33*, *34*). Because the force scales with the radius, very weak interactions of order kT are readily measured between the extended surfaces used with the SFA.

The adhesion energy density is determined from the force required to separate the surfaces or the pull-off force F_{po} and the JKR theory (*35*) for the adhesion between deformable surfaces. The JKR theory states that the adhesion energy per area and the pull-off force are related through $E_{area} = 2F_{po}/3\pi R$. In these measurements, F_{po} is the maximum attractive force measured at the point of adhesive failure and abrupt surface separation. Importantly, under near-equilibrium pulling conditions, F_{po} yields the adhesion energy directly.

Lipid Bilayer Deposition and Protein Immobilization. The supported lipid bilayers were prepared by the LB deposition of lipid monolayers from the water−air interface of a Langmuir trough (NIMA, Coventry, England) onto freshly cleaved mica supports, as described (*36*, *37*). The back surfaces of the mica sheets were coated with 500 Å reflecting silver layers, and the mica was glued silver side down onto a fused, hemicylindrical silica lens. The silica lenses were milled with 2 cm radii of curvature. The first, inner lipid layer was a monolayer of gel phase DPPE at a mean molecular area of 43 Å^2/lipid. The second, outer LB monolayer consisted of a mixture of either NTA-DLGE and DTPC or DSIDA and DSPC. The chain melting temperature of DTPC is 14 °C and that of DSPC is 55 °C, so that the resulting lipid mixtures were in the fluid and gel phase, respectively, at 25 °C. Two different lipid mixtures were used to generate fluid and gel phase monolayers. This was motivated in part by the requirements of miscibility of the lipid components at a variety of compositions and achieving both gel and fluid states over a limited range of temperatures. Studies with cadherin demonstrated that these different lipid

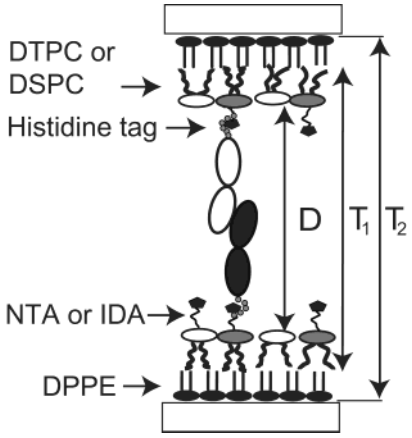

FIGURE 2: Illustration of the sample architecture used in the force measurements.

mixtures do not alter the bound protein orientation or function (*36*, *38*). However, consistent with previous work with streptavidin (*39*), the adhesion is expected to be higher on fluid membranes.

In both cases, the monolayers were deposited from the air−water interface at a surface pressure of 34 ± 1 mN/m. With the DTPC/NTA-DLGE monolayers this gave a mean molecular area of 60 ± 5 Å^2/lipid, and the average molecular area in the DSIDA/DSPC films was 45 ± 5 Å^2/lipid. The DSIDA/DSPC lipid films were deposited from an aqueous subphase containing 100 mM $NaNO_3$, 10 mM MOPS, 2 mM $Ca(NO_3)_2$, and 2 μM $Cu(NO_3)_2$ at pH 7.5, while a subphase of 100 mM $NaNO_3$, 10 mM MOPS, 2 mM $Ca(NO_3)_2$, and 25 μM $NiSO_4$ at pH 7.5 was used for the NTA-DLGE/DTPC lipid films. The subphases were maintained at 25 °C by a water jacket surrounding the trough.

Oriented CD2 and CD48 monolayers (Figure 2) were assembled by incubating the lipid bilayers with 5 μM His_6-CD2 or His_6-CD48 in the same buffer used in the subphase for the outer lipid monolayer described above. After 2 h incubation at room temperature, the samples were gently rinsed with a syringe using protein-free buffer to remove all nonspecifically adsorbed proteins. The protein-coated disks were then transferred under water and installed in the surface force apparatus.

Measurement of Protein Surface Density Using Surface Plasma Resonance. The protein surface densities bound to the DSIDA and NTA-DLGE lipid monolayers were estimated with a custom-built SPR instrument, described previously (*40*). The instrument consists of a precision goniometer (Oriel) driven by a stepper motor, an equilateral triangle prism, a large area Si photodiode, and a GaAs laser (5 mW, 665 nm) light source. A flow cell (volume ~0.5 mL) was used for the protein adsorption/desorption measurements.

For SPR measurements, the NTA-DLGE and DSIDA monolayers were supported on a self-assembled monolayer of 1-octadecanethiol on gold. The gold film was thermally evaporated onto a 10−15 Å chromium adhesion layer, which was evaporated onto a clean glass slide (*40*, *41*). In the protein adsorption experiments, the SPR cell containing the samples was first flushed with deionized water for 15 min at a rate of 10 mL/h. The IDA (or NTA) groups were then activated by flushing buffer containing 2 μM Cu^{2+} (or 25 μM Ni^{2+}) over the lipid monolayer for 10 min. The protein adsorption was initiated by injecting 2 mL of 5 μM CD2 or CD48 solution into the flow cell. After the substrates were incubated with the protein solution under stopped-flow conditions for about 2 h, the cell was flushed with buffer for 15 min at a rate of 10 mL/h. The change in the plasmon resonance angle $\Delta\theta_r$, resulting from the protein adsorption, was then converted to the change in the effective optical thickness of the protein layer Δnd, where n is the refractive index of the layer and d is the film thickness. This was accomplished with the Fresnel reflectivity equations. The lengths of the proteins are 75 Å, based on crystallographic data (*15*, *16*, *42*, *43*). The assumption that the proteins were oriented end-on was verified by the measured steric thickness of the protein layers determined from the force curves.

The fractional protein coverage x_p relative to a densely packed protein monolayer was then obtained using the measured value of the refractive index of the layer and $n = x_p n_p + (1 - x_p) n_{water}$. Here, the refractive index of the pure protein layer $n_p = 1.53$ and $n_{water} = 1.33$ is that of pure water. From the fractional protein coverage x_p and the known protein dimensions, we estimated the protein coverage in terms of the area per protein. All data were recorded at room temperature. The lower protein detection limit with this instrument is 0.02 mg m^{-2}, or 200 molecules/μm^2 for a protein with a molecular weight of 6 × 10^4.

Fluorescence Imaging of the Lipid Bilayers. Fluorescence microscopy was used to assess the lateral miscibility of the DSIDA (or NTA-DLGE) and DSPC (or DTPC). To visualize the lateral texture of the bilayer, 0.5 mol % of FITC-labeled DPPE was incorporated into the outer lipid monolayers. Studies were also done with labeled proteins to establish that they were homogeneously distributed on these membranes. The dye-labeled lipids were deposited onto freshly cleaved mica sheets that had been coated with a crystalline monolayer of DPPE and then transferred under water into a fluid cell designed for epifluorescence microscopy. The cell was filled with a 100 mM NaCl solution buffered with Tris (pH 7.1) and containing either 2 μM Cu^{2+} or 25 μM Ni^{2+}. Fluorescent micrographs were acquired using the same Olympus BX-60 microscope with an 80× objective (total magnification of 1400×).

RESULTS

Fluorescence Assay of the Miscibility of DTPC and DSIDA or NTA-DLGE. Fluorescence imaging microscopy showed that FITC-labeled DPPE distributes homogeneously in pure DTPC and in DSPC monolayers. The monolayers were structureless on a micron scale when either NTA-DLGE/DTPC or DSIDA/DSPC contained 25, 50, or 75 mol % NTA-DLGE or DSIDA. By contrast, DSIDA phase separated from DTPC at >50% DSIDA, and NTA-DLGE likewise did not mix with DSPC. The proteins that were bound to the homogeneously distributed NTA-DLGE and DSIDA monolayers were similarly homogeneously distributed.

Protein Surface Coverage Determined by SPR. Figure 3 shows a typical adsorption time course for CD2 binding to lipid membranes containing 25 mol % NTA-DLGE and 75 mol % of DTPC in the buffer described above. Upon injection of the bulk protein solution, the signal increases abruptly and plateaus after 10−15 min. After being rinsed with the identical buffer lacking protein, the amount of protein bound decreased slightly due to the removal of

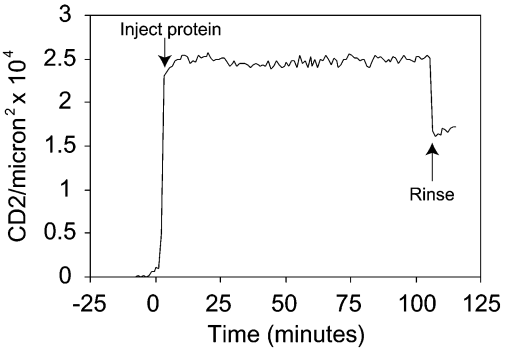

FIGURE 3: CD2 adsorption time course measured by surface plasmon resonance. The final total change in the signal indicates the total amount of protein specifically bound to the lipid surface. The supporting membrane contained 25 mol % NTA-DLGE and 75 mol % DTPC. The measurements were done at 25 °C in a solution containing 100 mM $NaNO_3$, 10 mM MOPS, 2 mM $Ca(NO_3)_2$, and 25 μM $NiSO_4$ at pH 7.5.

nonspecifically adsorbed protein. The shifts in the resonance angles were converted to protein surface densities (Figure 3) as described. Increasing the IDA or NTA content in the bilayer correspondingly increased the protein coverage (Table 1).

Surface Force Measurements: Definition of Zero Separation. In the measured force−distance profiles between CD2 and CD48 monolayers, the distance D (Figure 2) is the separation between the dehydrated surfaces of the matrix lipids that support the proteins. The bilayer separation D was determined by directly measuring the change in the total thickness T_1 of the organic layers between the DPPE monolayers following the deposition of the outer lipid layer and subsequent protein immobilization. Thus, $D = T_1 - 2T_{DTPC}$, where T_{DTPC} is the 16 Å thickness of the DTPC lipid layer determined in independent measurements. When DSPC was used as the matrix, the monolayer thickness was 27 Å (*37*). Alternatively, at the end of each measurement, the total thickness T_2 of all the organic layers between mica substrates was determined from the change in the distance of closest intersurface approach before and after removal of all the organic layers by UV irradiation (*44*, *45*), after the buffer in the SFA was drained. In this case, $D = T_2 - 2T_{DPPE} - 2T_{DTPC}$, where T_{DPPE} is the 25 Å thickness of DPPE monolayer (*37*). The measured thicknesses of the lipid, protein, and polymer layers determined by these methods have been shown to agree quantitatively with crystallographic data and with X-ray and neutron reflectivity data (*37*, *44*, *46*−*51*). Additionally, in this study, the values of D obtained with both of these methods agreed with each other within ±2 Å.

Adhesion between CD2 and CD48 on Fluid Membranes. The force profiles between CD2 and CD48 monolayers bound to fluid NTA-DLGE/DTPC membranes are shown in Figure 4. Data were obtained with 25 and 75 mol % NTA-DLGE membranes. When the outer monolayer contained 25 mol % NTA-DLGE, the CD2 and CD48 surface densities were 1.7×10^4 and 2.4×10^4 proteins/μm^2, respectively. The onset of steric repulsion between these protein monolayers occurs at D <170 Å. Upon separation (increasing D) there is a pronounced hysteresis between the forces measured during approach (advancing) and those measured during separation (receding). In addition, at the minimum in the force curve (maximum attractive force) at 152 ± 3 Å, the protein−protein bonds yield and the surfaces jump out of adhesive contact. The normalized adhesive force is weak at $F_{po}/R = -0.37 \pm 0.07$ mN/m.

Using JKR theory and F_{po}, the calculated adhesion energy per area is $E = F_{po}/1.5\pi R = 0.08$ mJ/m^2 (*52*). This is on the order of the measured van der Waals attraction between phosphatidylcholine bilayers in aqueous solutions (*37*). By normalizing this value by the density of CD2 (lower coverage), we estimated the average adhesion energy per heterophilic protein pair.

These normalized force−distance curves were reproducible. If the forces were remeasured immediately after pull-off, then the force profile was identical to that of the previous measurement. This indicated that there were no irreversible changes due to the rupture of the NTA/histidine bond or to the pull-out of the lipid anchors (*39*). As we demonstrated previously (*39*), such changes irreversibly damage the surfaces and alter the interaction profiles. The proteins pulled to the opposite surface would increase the range and magnitude of the repulsion between the two membranes, relative to the undamaged layers (*39*). Moreover, in this study, the forces measured were well below the level required for lipid extraction at these loading rates (*39*).

The adhesion increased with the protein surface density (Figures 4 and 5). When 75 mol % NTA/25 mol % DTPC was used as the outer lipid layer, the CD2 and CD48 surface densities increased to 6.3×10^4 molecules/μm^2 and 6.9×10^4 molecules/μm^2, respectively (Table 1). The range of the repulsion did not change, but the magnitude of the steric and osmotic repulsion between the membranes increased, as expected (Figure 4). Most importantly, the magnitude of the adhesion increased 3-fold to −1.31 ± 0.16 mN/m (0.23 mJ/m^2) (Table 1). Nevertheless, the position of the adhesive minimum was unchanged at 153 ± 5 Å (Figure 4).

Measurements between the bare lipid membranes without attached proteins exhibit electrostatic repulsion in the buffers used in these experiments. However, the range of the double layer repulsion is <25 Å between, for example, membranes comprising 25 mol % of NTA-DLGE and 75% DTPC. In all cases, the range of the repulsion was less than the 153 Å range of protein−protein attraction.

An important characteristic of the measured adhesion between CD2 and CD48 monolayers is the dependence of adhesion energy on the contact time between the two surfaces. As Figure 5 shows, the adhesion energy increases upon prolonged membrane contact. The data shown were obtained by conducting sequential measurements in which the contact time was varied randomly between 1 and 30 min. Thermal drifts amount to <0.1 mN/m during the 30 min incubation. There were no changes observed between any two successive force measurements. This indicates that the increase in adhesion was due to a time-dependent increase in the number of protein molecules engaged in binding interactions. At both protein densities examined, the adhesion energy appeared to plateau after the surfaces were kept in contact for about 10 min. The estimated average adhesion energy per protein pair, determined from the pull-off force at the plateau, was ∼1 kT at 25 °C.

CD2 and CD48 Immobilized on Gel Phase Lipids. Force distance profiles between CD2 and CD48 immobilized on gel phase membranes containing 75 mol % DSIDA and 25

Table 1: Adhesion as a Function of the Protein Coverage and Membrane Fluidity

composition of outer lipid layer	protein surface density (molecules/μm^2) CD2	CD48	minimum (Å)	adhesion (mN/m)	estimated energy per bond (kT)
25% NTA/75% DTPC	1.7×10^4	2.4×10^4	152 ± 3	-0.38 ± 0.07	1
75% NTA/25% DTPC	6.3×10^4	6.9×10^4	153 ± 5	-1.31 ± 0.16	1
75% IDA/25% DSPC	6.4×10^4	4.8×10^4	153 ± 3	-0.13 ± 0.03	0.01

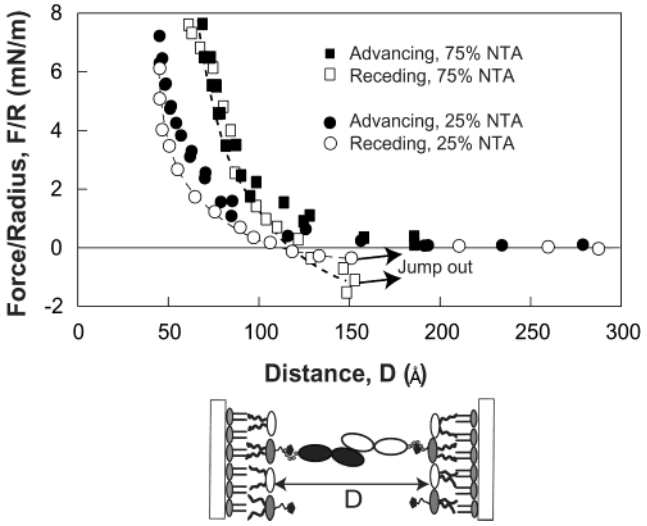

FIGURE 4: Force versus distance profiles between CD2 and CD48 monolayers on lipid bilayers containing NTA-DLGE and DTPC. Circles indicate measurements done with membranes containing 25 mol % NTA-DLGE, and squares indicate the measurements done with 75 mol % NTA-DLGE membranes. The protein surface densities on each of these membranes are summarized in Table 1. The curves show the adhesion measured after the protein layers were left in contact for 10 min. The outward directed arrows indicate the position at which the surfaces jumped out of adhesive contact.

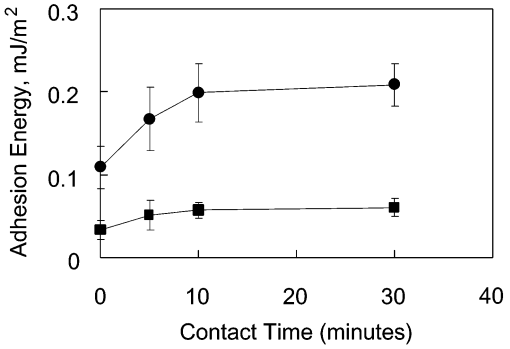

FIGURE 5: Dependence of the adhesion energy per area on the contact time between fluid membranes. The percentages of NTA-DLGE and DTPC in the outer layer were 25 mol % (squares) and 75 mol % (circles). The force profiles were measured between CD2 and CD48 membranes at 25 °C in a solution containing 100 mM $NaNO_3$, 10 mM MOPS, 2 mM $Ca(NO_3)_2$, and 25 μM $NiSO_4$ at pH 7.5.

mol % DSPC are shown in Figure 6. As with fluid membranes, there was no measured force at $D > 180$ Å, and the onset of intersurface repulsion occurs at ~170 Å. There was weak adhesion between CD2 and CD48 monolayers bound to gel phase lipids (Table 1). The maximum attraction was at 152 ± 5 Å, but the magnitude of the adhesion was significantly lower at -0.13 ± 0.03 mN/m (0.03 mJ/m^2). In contrast to measurements with fluid membranes, the adhesion did not increase with the time in contact. The latter finding

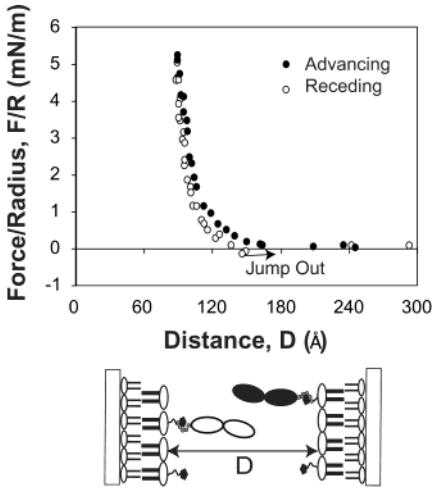

FIGURE 6: Force−distance profiles between CD2 and CD48 monolayers on lipid membranes comprising 25 mol % DSIDA and 75 mol % DSPC. The protein surface densities were 2.0×10^4 and 1.4×10^4 molecules/μm^2 for CD2 and CD48, respectively. The advancing (filled circles) and receding (open circles) force profiles were measured at 25 °C in a solution containing 100 mM $NaNO_3$, 20 mM MOPS, 2 mM $Ca(NO_3)_2$, and 2 μM $CuSO_4$ at pH 7.5.

confirms that the time-dependent increase in adhesion on fluid lipid bilayers is due to increased lateral and rotational mobility.

Homophilic Interactions Do Not Generate Adhesion. Figure 7 shows the results of control measurements between identical CD48 monolayers on fluid membranes (75 mol % NTA-DLGE). The CD48 surface coverage was 6.9×10^4 molecules/μm^2. The advancing and receding force profiles were identical, and there was no adhesion, even when the protein monolayers remained in contact for up to 30 min. Interestingly, the force profiles between CD2 monolayers did display some hysteresis, but no adhesion, between the advancing and receding curves (data not shown).

DISCUSSION

This study demonstrates the use of direct force−distance measurements to determine the molecular mechanism of adhesion protein interactions. In particular, the position of the adhesive minimum in the force−distance curves demonstrates directly that CD2 and CD48 adhere in a head-to-head orientation. The single angstrom resolution in the measured intersurface spacing allows the determination of the absolute end-to-end distance at which CD2 and CD48 bind. One of the more important advantages of the SFA relative to other force probes is that, with the in situ interferometric technique, the SFA measurements yield the *absolute distances* (not relative distances) within ±1 Å between the materials under investigation (*53*). Moreover, coupling this distance resolution with direct measurements of the adhesive function allows questions regarding the

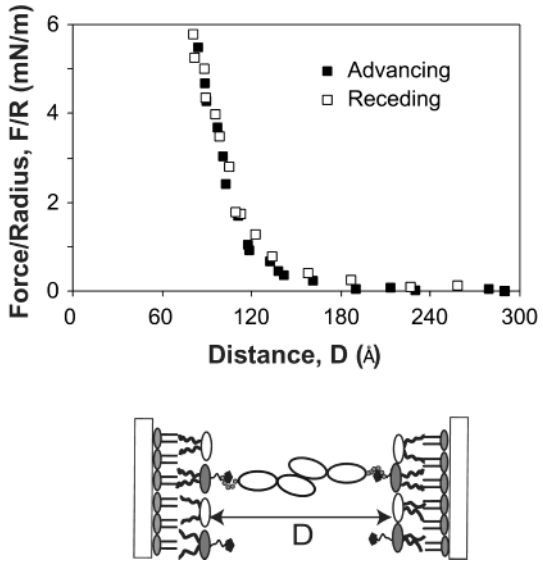

FIGURE 7: Force versus distance profiles between identical CD48 monolayers on fluid lipid membranes. The supporting membranes contained 75 mol % NTA-DLGE. The advancing (filled squares) and receding (open squares) force profiles were measured with a CD48 surface coverage of 6.9×10^4 molecules/μm^2 at 25 °C. The bathing solution contained 100 mM $NaNO_3$, 10 mM MOPS, 2 mM $Ca(NO_3)_2$, and 25 μM $NiSO_4$ at pH 7.5.

relative binding orientations of proteins forming the adhesive complex to be directly addressed.

In these SFA measurements, the range of the steric repulsion between the protein layers (D <170 Å) agrees quantitatively with that expected on the basis of the 75 Å lengths of both CD2 and CD48 (*42*, *54*) as well as the measured 10 Å lengths of the NTA and IDA spacers [$D = 2(75 + 10$ Å)] (*36*, *38*). The proteins are therefore oriented end-on at the membrane surface, so that the binding sites are presented to the opposite membrane as on the cell surface.

In force measurements between the CD2 and CD48 on fluid membranes, the measured adhesive minimum was at a bilayer−bilayer separation of $D = 153 \pm 5$ Å. The independence of both the onset of the repulsion and the position of the adhesive minimum on the protein density also demonstrates that the protein surface density does not affect either the protein orientation or the range of the protein−protein attraction. Accounting for the 10 Å length of the NTA tether, this shows that proteins adhere at an end-to-end distance of 133 ± 5 Å. The measured range of protein binding agrees quantitatively with the predicted end-to-end distance of 134 Å for the heterophilic CD2−CD48 complex (*6*, *55*). The *predicted* binding mechanism was based on a model derived from the (i) crystal structure of CD2, (ii) the demonstration, by complementary mutagenesis, that CD2 interacts with CD48 in the same head-to-head orientation as the homophillic interaction observed in CD2 crystals (*55*), and (iii) the published structure of the complex formed by the outer domain fragments of CD2 and CD58, the human homologue of CD48 (*19*). The homology with CD58 suggested that CD48 would similarly bind CD2. These direct force measurements with the SFA confirm the model and at the same time show that such measurements can provide direct evidence for protein docking orientations.

These results also provide direct evidence that the CD2−CD48 interaction spans a distance similar to the dimensions of the TCR/peptide−MHC complex (130−135 Å) (*6*). This direct demonstration that CD2 interacts with its ligand CD48 in the same orientation as CD2 and CD58 suggests that CD2−ligand interactions may all span a similar intermembrane distance. It was postulated that CD2−ligand binding positions the membranes of the T cell and APC at a separation distance optimal for TCR engagement of MHC−peptide complexes (*42*). The present study confirms that the CD2−CD48 interaction would indeed position membranes at the optimum distance for this function.

The CD2−CD48 bond fails abruptly from the position of head-to-head contact. The structures of both CD2 and CD58 revealed that the IgV-type structure of domain 1 of both proteins lacks a disulfide bond (*19*). It was suggested that this might impart elasticity to adhesive junctions. Others similarly hypothesized that forced domain unfolding might play a role in the function of IgSF adhesion proteins (*56*). Molecular extension over a range of >5 Å would be evident in the force−distance profiles, as has been observed previously with the SFA (*57*−*59*). The 20° range of motion about the domain 1−domain 2 linker (*19*, *54*) accounts for the ±5 Å variation in the measurements, but there was no evidence of any elastic extension of the proteins during unbinding. Given the large forces typically required to unfold protein domains (*60*, *61*) and the very weak heterophilic bonds measured in this study, it is unlikely that unfolding transitions play a role in CD2 or CD48 function; that is, the heterophilic protein−protein bonds will rupture before the domains unfold.

The binding interface of the CD2−CD58 complex contains several charged residues that participate in salt bridges between the two, broad binding surfaces of the β-sheets (*6*, *19*). Because the CD2−CD48 adhesive complex involves slightly fewer such contacts (*6*, *14*), the ionic complementarity was proposed to confer binding specificity (*14*). The force−distance profiles confirm the absence of a long-range electrostatic attraction between CD2 and CD48, even at lower ionic strength (data not shown). The CD2/CD48 binding affinity is also ionic strength independent (*62*). By contrast, fluorescein association with 4-4-20 antifluorescein Fab′ is ionic strength dependent. The latter is attributed to the charge cluster surrounding the Fab′ binding site, which was shown, by surface force measurements, to generate a long-range electrostatic attraction between the Fab′ and fluorescein-coated membranes (*48*). The lack of any long-range electrostatic attraction supports the hypothesis that salt bridges only affect short-range CD2−CD48 interactions.

Homophilic head-to-head CD2−ligand binding was suggested by the dimer-like structure of CD2 in its crystalline form (*15*, *16*). The lack of CD48−CD48 binding demonstrates the specificity of the heterophilic CD2−CD48 bond. Very weak homophilic CD2 attraction, suggested by the slight hysteresis in the force curves between CD2 monolayers, is plausible. Both rat and human CD2 crystallized with the same homophilic contacts as at the interfaces with CD48 and CD58. Other members of the CD2 family such as SLAM undergo homophilic binding (*63*). NMR studies suggested that murine CD2 self-associates with a millimolar dissociation constant (*64*). Nevertheless, there is no evidence that either CD2 or CD48 interacts homotypically under physiological conditions (*1*), and these direct measurements confirm that it would not occur.

The low measured heterotypic adhesion demonstrates the inherently weak nature of the CD2−CD48 bond. From SPR studies, the measured affinity constant between CD2 and CD48 in solution is around 10^4 M^{-1}, and the dissociation rates are 7.8 s^{-1} (*12*−*14*, *62*). In these SFA measurements, the estimated average adhesion energy per CD2−CD48 pair on fluid membranes (Table 1) is ∼1 kT, regardless of the protein surface density. This is much lower than the estimated 8 kT determined with the protein C-cadherin, similarly bound to fluid NTA-DLGE membranes (*38*). At comparable protein densities and pulling rates, cadherin adhesion is nearly an order of magnitude larger. Cadherin is a stronger adhesion protein since homophilic cadherin binding aggregates beads but heterophilic CD2 and CD48 interactions do not. This could be due to the differences in protein dimensions, since cadherin is larger, more flexible, and may exhibit a larger reactive cross section. On the other hand, unlike the mechanically important cadherin binding, which enables cells to associate into tissues, the interaction of the T lymphocyte adhesion molecule CD2 with its ligand CD48 on APC's functions mainly to enhance recognition of antigen on APC's by the TCR. Since the surface density of *specific* peptide−MHC, which can engage the TCR, is usually very low (<0.1% of all peptide−MHC), rapid lateral diffusion of peptide−MHC through the T cell−APC contact area is presumably important for TCR engagement. The low adhesion energy and fast dissociation rate may be required to allow lateral diffusion through the contact interface formed by CD2−CD48 interactions.

Such low-affinity bonds necessitate the accumulation of multiple protein−protein contacts (*21*, *22*, *65*) to generate adhesion energies $>kT$ between cells. The importance of lateral mobility for the development of appreciable CD2−CD48 adhesion was demonstrated with fluid versus gel phase lipid membranes. The reduced mobility restricts binding to the few proteins initially in register upon membrane contact, and this lowered the adhesion between gel phase membranes 10-fold, even at the highest CD2 surface densities of 6.9×10^4 molecules/μm^2. The estimated CD2 density of ∼110 molecules/μm^2 on T cells is more than 2 orders of magnitude lower than used in these investigations. Here, the measured adhesion energy between protein monolayers on fluid lipids is only 2−3 times greater than the van der Waals attraction between phosphatidylcholine membranes. That CD2 is present at much lower densities on T cells further supports the conclusion that protein enrichment at contact sites is essential for mediating cell−cell adhesion with these weak heterophilic bonds. These results agree qualitatively with the temperature dependence of Jurkat cell adhesion to planar bilayers displaying CD58 (LFA-3) (*22*). The temperature reductions used in the latter study (*66*) can cause other physiological changes, but these direct measurements confirm that limiting bond accumulation at contact sites substantially reduces the adhesion mediated by these weakly binding proteins.

In conclusion, we used direct, molecular force measurements to probe the relationships between the structures of CD2 and its ligand CD48, the mechanism of adhesion, and the strength of adhesion mediated by these heterotypic interactions. The force measurements directly confirm that the full-length extracellular regions of CD2 and CD48 bind in a head-to-head orientation. The absence of long-range electrostatic attraction shows further that salt bridges at the binding interface only influence short-range (<10 Å) interactions. Direct measurements also confirm that the adhesion mediated by the low-affinity CD2−CD48 is very weak. As a result, lateral mobility and the accumulation of multiple intersurface bonds are necessary for the development of physiologically significant adhesion. As the first direct, molecular force measurements of the heterotypic adhesion between cell adhesion proteins, these findings demonstrate the potential of this approach for probing the molecular mechanisms underlying adhesion protein function.

ACKNOWLEDGMENT

We thank Alice Kearney for help with the preparation of recombinant proteins.

REFERENCES

1. van der Merwe, P. A., McPherson, D. C., Brown, Barclay, A. N., Cyster, J. G., Williams, A. F., and Davis, S. J. (1993) *Eur. J. Immunol. 23*, 1373−1377.
2. Springer, T. A. (1990) *Nature 341*, 619−621.
3. Davis, S. J., and van der Merwe, P. A. (1996) *Science 273*, 1241−1242.
4. Hunig, T. (1985) *J. Exp. Med. 162*, 890−901.
5. Kato, K., Koyanagi, M., Okada, H., Takanashi, T., Wong, Y. W., Williams, A. F., Okumura, K., and Yagati, H. (1992) *J. Exp. Med. 176*, 1241−1249.
6. Davis, S., Ikemizu, S., Wild, M. K., and van der Merwe, P. A. (1998) *Immunol. Rev. 163*, 217−236.
7. Peterson, A., and Seed, B. (1987) *Nature 329*, 846−848.
8. Seed, B. (1987) *Nature 329*, 840−842.
9. Dustin, M. L., Selveraj, P., Mattaliano, R. J., and Springer, T. A. (1987) *Nature 329*, 846−848.
10. Sewell, W., Brown, M. H., Dunne, J., Owen, M. J., and Crumpton, M. J. (1986) *Proc. Natl. Acad. Sci. U.S.A. 83*, 8718−8722.
11. Williams, A., Barclay, A. N., Clark, S. J., Paterson, D. J., and Willis, A. C. (1987) *J. Exp. Med. 165*, 368−380.
12. Pierres, A., Benoliel, A. M., Bongrand, P., and van der Merwe, A. P. (1996) *Proc. Natl. Acad. Sci. U.S.A. 93*, 15114−15118.
13. van der Merwe, P. A., Barclay, A. N., Mason, D. W., Davies, E. A., Morgan, B. P., Tone, M., Krishnam, A. K. C., Ianelli, C., and Davis, S. J. (1994) *Biochemistry 33*, 10149−10160.
14. Davis, S. J., Davies, E. A., Tucknott, M. G., Jones, E. Y., and van der Merwe, A. (1998) *Proc. Natl. Acad. Sci. U.S.A. 95*, 5490−5494.
15. Jones, E., Davis, S. J., Williams, A. F., Harlos, K., and Stuart, D. I. (1992) *Nature 360*, 232−239.
16. Bodian, D., Jones, E. Y., Stuart, D. I., Harlos, K. H., Davis, E. A., and Davis, S. J. (1994) *Structure 2*, 755−766.
17. McAlister, M., Moss, H. R., van der Merwe, P. A., Campbell, I. D., Davis, S. J., and Driscoll, P. C. (1996) *Biochemistry 35*, 5982−5991.
18. Ikemizu, S., Sparks, L. M., van der Merwe, P. A., Harlos, K., Stuart, D. I., Jones, E. Y., and Davis, S. J. (1999) *Proc. Natl. Acad. Sci. U.S.A. 96*, 4289−4294.
19. Wang, J., Smolyar, A., Tan, K., Liu, J. H., Kim, M., Sun, Z. J., Wagner, G., and Reinherz, E. L. (1999) *Cell 97*, 791−803.
20. Pierres, A., Benoliel, A. M., Bongrand, P., and van der Merwe, P. A. (1997) *FEBS Lett. 403*, 239−244.
21. Dustin, M. L., Golan, D. E., Zhu, D.-M., Miller, J. M., Meier, W., Davies, E. A., and van der Merwe, P. A. (1997) *J. Biol. Chem. 272*, 30889−30898.
22. Dustin, M. L. (1997) *J. Biol. Chem. 272*, 15782−15788.
23. Grakoui, A., Bromley, S. K., Sumen, C., Davis, M. M., Shaw, A. S., Allen, P. M., and Dustin, M. L. (1999) *Science 285*, 221−226.
24. Qi, S., Groves, J. T., and Chakraborty, A. K. (2001) *Proc. Natl. Acad. Sci. U.S.A. 98*, 6548−6553.
25. Merkel, R., Nassoy, P., Leung, A., Ritchie, K., and Evans, E. (1999) *Nature 397*, 50−53.
26. Evans, E., and Ritchie, K. (1997) *Biophys. J. 72*, 1541−1555.
27. Vijayendran, R., Hammer, D., and Leckband, D. (1998) *J. Chem. Phys. 108*, 7783−7793.

28. Seifert, U. (2000) *Phys. Rev. Lett. 84*, 2750−2753.
29. van der Merwe, P., Bodian, D. L., Daenke, S., Linsley, P., and Davis, S. J. (1997) *J. Exp. Med. 185*, 393−403.
30. Israelachvili, J., and McGuiggan, P. (1990) *J. Mater. Res. 5*, 2223−2231.
31. Israelachvili, J. (1973) *J. Colloid Interface Sci. 44*, 259−272.
32. Derjaguin, B. V. (1934) *Kolloid-Z. 69*, 155−164.
33. Hunter, R. (1989) *Foundations of Colloid Science*, Vol. 1, Oxford University Press, Oxford.
34. Israelachvili, J. (1992) *Surf. Sci. Rep. 14*, 110−159.
35. Johnson, K. L., Kendall, K., and Roberts, A. D. (1971) *Proc. R. Soc. London, Ser. A 324*, 301−313.
36. Sivasankar, S., Gumbiner, B., and Leckband, D. (2001) *Biophys. J. 80*, 1758−1768.
37. Marra, J., and Israelachvili, J. (1985) *Biochemistry 24*, 4608−4618.
38. Sivasankar, S., Brieher, W., Lavrik, N., Gumbiner, B., and Leckband, D. (1999) *Proc. Natl. Acad. Sci. U.S.A. 96*, 11820−11824.
39. Leckband, D., Müller, W., Schmitt, F.-J., and Ringsdorf, H. (1995) *Biophys. J. 69*, 1162−1169.
40. Lavrik, N., and Leckband, D. (2000) *Langmuir 16*, 1842−1851.
41. Zhu, B., Eurell, T., Gunawan, R., and Leckband, D. (2000) *J. Biomater. Sci., Polym. Ed. 56*, 406−416.
42. Davis, S. J., and van der Merwe, P. A. (1996) *Immunol. Today 17*, 177−187.
43. Driscoll, P. C., Cyster, J. G., Campbell, I. D., and Williams, A. F. (1991) *Nature 353*, 762−765.
44. Leckband, D., Schmitt, F.-J., Israelachvili, J., and Knoll, W. (1994) *Biochemistry 33*, 4611−4624.
45. Leckband, D. E., Helm, C. A., and Israelachvili, J. (1993) *Biochemistry 32*, 1127−1140.
46. Mohwald, H. (1990) *Annu. Rev. Phys. Chem. 41*, 441−476.
47. Johnson, S. J., Bayerl, T. M., McDermott, D. C., Adam, G. W., Rennie, A. R., Thomas, R. K., and Sackmann, E. (1991) *Biophys. J. 59*, 289−294.
48. Leckband, D. E., Kuhl, T. L., Wang, H. K., Müller, W., and Ringsdorf, H. (1995) *Biochemistry 34*, 11467−11478.
49. Yeung, C., Purves, T., Kloss, A., Sligar, S., and Leckband, D. (1999) *Langmuir 15*, 6829−6836.
50. Kuhl, T. L., Majewski, J., Wong, J. Y., Steinberg, S., Leckband, D. E., Israelachvili, J. N., and Smith, G. S. (1998) *Biophys. J. 75*, 2352−2362.
51. Majewski, J., Kuhl, T., Kjaer, K., Gerstenberg, M. C., Als-Nielsen, J., Israelachvili, J. N., and Smith, G. S. (1998) *J. Am. Chem. Soc. 120*, 1469−1473.
52. Israelachvili, J. (1991) *Intermolecular and Surface Forces*, 2nd ed., Academic Press, New York.
53. Leckband, D., and Israelachvili, J. (2001) *Q. Rev. Biophys. 34*, 105−267.
54. Yvonne Jones, E., Davis, S. J., Williams, A. F., Harlos, K., and Stuart, D. I. (1992) *Nature 360*, 232−239.
55. van der Merwe, P., McNamee, P. N., Davies, E. A., Barclay, A. N., and Davis, S. J. (1995) *Curr. Biol. 5*, 74−84.
56. Fisher, T. E., Carion-Vasquez, M., Oberhauser, A. F., Li, H. B., Marszalek, P. E., and Fernandez, J. M. (2000) *Neuron 27*, 435−446.
57. Wong, J. Y., Kuhl, T. L., Israelachvili, J. N., Mullah, N., and Zalipsky, S. (1997) *Science 275*, 820−822.
58. Jeppsesen, C., Wong, J. Y., Kuhl, T. L., Israelachvili, J. N., Mullah, N., Zalipsky, S., and Marques, C. M. (2001) *Science 293*, 465−468.
59. Yu, Z.-W., Calvert, T., and Leckband, D. (1998) *Biochemistry 37*, 1540−1550.
60. Kellermayer, M., Smith, S. B., Granzier, H. L., and Bustamante, C. (1997) *Science 276*, 1112−1115.
61. Rief, M., Gautel, M., Oesterhelt, F., Fernandez, J. M., and Gaub, H. E. (1999) *Science 276*, 1109−1112.
62. van der Merwe, P. A., Brown, M. H., Davis, S. J., and Barclay, N. A. (1993) *EMBO J. 12*, 4945−4954.
63. Mavaddat, N., Mason, D. W., Atkinson, P. D., Evans, E. J., Gilbert, R. J. C., Stuart, D. I., Gennelly, J. A., Barclay, A. N., Davis, S. J., and Brown, M. H. (2000) *J. Biol. Chem. 275*, 28100−28109.
64. Pfuhl, M., Chen, H. A., Kristensen, S. M., and Driscoll, P. D. (1999) *J. Biomol. NMR 14*, 307−320.
65. Dustin, M. L., Ferguson, L. M., Chan, P.-Y., Springer, T. A., and Golan, D. E. (1996) *J. Cell Biol. 132*, 465−474.
66. Chan, P.-Y., Lawrence, M. B., Dustin, M. L., Ferguson, L. M., Golan, D. E., and Springer, T. A. (1991) *J. Cell Biol. 115*, 245−255.

BI020296G